Magnons and fractons in the diluted antiferromagnet $Mn_xZn_{1-x}F_2$

Y. J. Uemura
Brookhaven National Laboratory, Upton, New York 11973

R. J. Birgeneau
Department of Physics, Massachusetts Institute of Technology, Cambridge, Massachusetts 02139
(Received 24 April 1987)

We report high-resolution inelastic-neutron-scattering studies of the spin dynamics in the diluted near-Heisenberg antiferromagnet $Mn_xZn_{1-x}F_2$ with $x=0.75$ and 0.50. The $x=0.75$ experiments reproduce previous results by Coombs *et al.* [J. Phys. C **9**, 2167 (1976)], albeit with much higher resolution. In that case the excitations may be described as spin waves which broaden progressively as the wave vector approaches the zone-boundary value q_{ZB}. However, even at q_{ZB} the excitation is underdamped. More interesting behavior is observed in the $x=0.50$ sample. At long wavelengths, the response function $S(\mathbf{q},\omega)$ is dominated by a sharp spin-wave peak; however, there is a weak ω^{-3} tail extending to high energies. With increasing wave vector the sharp peak diminishes in intensity while a broad overdamped component, which is well described by a damped-harmonic-oscillator (DHO) function, grows in intensity. The crossover from a dominant spin wave to a dominant DHO response occurs for $q\sim 0.3q_{ZB}$. In energy space, this phenomenon manifests itself as a crossover from propagating low-energy spin waves to localized high-energy excitations. An independent measurement of elastic diffuse magnetic scattering from the $x=0.50$ sample yields the percolation correlation length ξ_p associated with the dilution as $\xi_p^{-1}=0.3q_{ZB}$. This demonstrates that the crossover in the dynamics occurs at the length scale characteristic of the static geometrical disorder. The results are thence related to the magnon-fracton crossover predicted by recent theories for percolation networks.

I. INTRODUCTION

There has been continued development in research on disordered systems in recent years.[1-3] Among the most extensively investigated experimental systems are the randomly diluted antiferromagnets $Mn_xZn_{1-x}F_2$ and $Fe_xZn_{1-x}F_2$; these materials are characterized by randomness due purely to the geometry of the spin network; they form a group of materials distinguished from other magnetically disordered systems such as spin glasses where the spin frustration makes the situation more complicated and specifically where nonequilibrium effects play an essential role. Experiments on randomly diluted antiferromagnets have been extensively performed with a variety of interests including the spin dynamics,[4,5] critical behavior,[6,7] percolation,[8,9] and random-field effects.[10]

On the theoretical side, an interesting new development has been the introduction of the concept of "fractals."[11] This has opened up a novel geometrical approach in the treatment of randomness in physical systems.[12] Theoretical studies have then been extended to characterize the dynamic excitations in such random media.[3,13-18] Specifically, it has been predicted that in a percolation network, propagating phonons or magnons at long wavelengths and low energies should cross over to localized "fracton" excitations at higher energies and shorter length scales where the network has a fractal geometry.

Based on this picture, the density of states was derived for phonon (or magnon) and fracton excitations, and the results have been employed to explain the temperature dependence of the specific heat of epoxy resins[19] and the thermal conductivity of glassy systems.[20] The application of fractal concepts to these dense systems is not without controversy. Nevertheless, it is evident that a wide range of physical phenomena in disordered systems might be understood via the novel fracton conjecture. There has been, however, no clear microscopic experimental observation of the anticipated crossover phenomena in random magnetic systems. It is therefore a challenge for scattering experiments to measure the propagation and damping of phonons or magnons in model random systems exhibiting fractal geometry at short length scales and to characterize the detailed aspects of the dynamic excitations.

In this paper, we give a full description of our inelastic-neutron-scattering experiments on the site-diluted random antiferromagnet $Mn_xZn_{1-x}F_2$. By diluting the ionic antiferromagnet MnF_2 one produces a randomly diluted antiferromagnet $Mn_xZn_{1-x}F_2$. MnF_2 is a representative three-dimensional Heisenberg antiferromagnet with the rutile structure as shown in Fig. 1, and has been studied by many different experimental methods.[21] The dipolar interaction between the Mn moments accounts for a weak Ising anisotropy which aligns the Mn spins along the c axis below the Néel temperature $T_N=67.4$ K. The antiferromagnetic exchange interaction is much stronger than the anisotropy energy, and thus the system is dominated by the Heisenberg in-

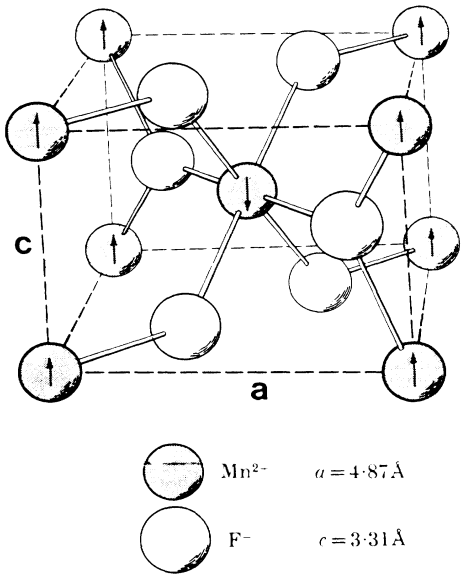

FIG. 1. Crystal structure of MnF_2. Mn moments in the tetragonal rutile-type crystal order antiferromagnetically along the c axis below the Néel temperature $T_N=67.4$ K.

teraction which supports spin-wave excitations below T_N. The energy of magnons in pure MnF_2 is ~ 6.5 meV at the zone boundary, while the Ising gap at the zone center is 1.08 meV.[22]

The antiferromagnetic exchange interaction between neighboring Mn moments on different sublattices, that is, between the Mn moments placed at the body center and the corner of the rutile crystal is much stronger than the coupling between Mn spins on the same sublattice. Thus the replacement of Mn atoms with nonmagnetic Zn atoms simply changes the geometry of the magnetic spin network, but does not introduce any spin frustration. This is in contrast to the case of $Eu_xSr_{1-x}S$, where the comparable strength but opposite signs of the first- and second-neighbor exchange results in a serious spin frustration which leads to the spin-glass properties.[23] In $Mn_xZn_{1-x}F_2$, the Zn atoms are assumed to replace Mn randomly, as is supported by NMR (Ref. 24) and diffuse-neutron-scattering measurements.[25] All these characteristics make $Mn_xZn_{1-x}F_2$ an ideal system which is directly comparable to the three-dimensional body-centered-cubic percolation spin network.[1,26] The percolation threshold x_p is at 25% Mn concentration ($x_p=0.25$).

The problem of antiferromagnetic spin waves maps onto the problem of phonons, because both excitations have dispersion linear in the wave vector at long wavelengths. Therefore, the study of the dynamic spin excitations in $Mn_xZn_{1-x}F_2$ should also elucidate the behavior of the lattice vibrations in disordered solids. An important feature of the $Mn_xZn_{1-x}F_2$ system is that the quality of the crystals has been improved markedly in recent years. High-quality single crystals can now be obtained with a homogeneous Mn concentration within a large volume. The availability of high-quality single crystals is especially important for scattering studies of the dynamic excitations.

Neutron scattering measurements on the spin waves in $Mn_xZn_{1-x}F_2$ were previously reported by Coombs *et al.*[4] and by Dietrich *et al.*[5] Coombs *et al.*[4] performed inelastic scattering studies on single crystals of $Mn_{0.78}Zn_{0.22}F_2$ and $Mn_{0.32}Zn_{0.68}F_2$ from the center to the boundary of the antiferromagnetic Brillouin zone. In the magnetically concentrated 78% sample, they observed well-defined spin waves throughout the Brillouin zone. The energy width of the spin-wave signal broadened with increasing wave vector, but the full width was still only one-half of the peak energy even at the zone boundary. In contrast, for the $Mn_{0.32}Zn_{0.68}F_2$ sample which was close in concentration to the percolation threshold $x_p=0.25$, a very broad response was observed even near the zone center with no evidence for propagating spin waves. The experiment by Dietrich *et al.*[5] on $Mn_{0.68}Zn_{0.32}F_2$ was performed only at the zone boundary. Their motivation was to search for possible structure in the response function arising from the local atomic environment. Some indication of such structure was indeed found in the energy spectrum, although it represented a quite subtle feature.

We have performed high-resolution inelastic scattering measurements on $Mn_xZn_{1-x}F_2$ by using neutrons from the High Flux Beam Reactor of Brookhaven National Laboratory. A high-quality single crystal of quite large size (~ 10 cm^3) was grown at Massachusetts Institute of Technology (MIT) by D. Gabbe and A. Linz. The large volume of this crystal enabled us to perform detailed measurements with an instrumental energy resolution much better than that used in the previous experiments of Coombs *et al.*[4] As reported in the brief letter[27] which introduced part of the present study, we found sharp spin waves near the zone center, rapid broadening of the energy spectrum with increasing wave vector q, and broad excitations at higher energies whose energies and widths depended only weakly on q. These features demonstrate a crossover from propagating spin waves to localized excitations. We describe full details of this experiment here together with some results on $Mn_{0.75}Zn_{0.25}F_2$ which we obtained for the purpose of comparison with the 50% specimen. We also describe elastic magnetic diffuse scattering measurements in $Mn_{0.5}Zn_{0.5}F_2$ which separates the region of Euclidean and fractal geometry in the percolation network.

The paper is organized in the following way. We will first present results from the inelastic-neutron-scattering study in Sec. II with the data essentially unprocessed so that one may discuss the essential qualitative features of the experiment. In Sec. III, we discuss the stiffness of low-energy spin waves in terms of the percolation problem. We also provide a brief review of the fracton picture. The diffuse-neutron-scattering results are presented in Sec. IV. In Sec. V we will present a detailed analysis of the line shapes of the inelastic energy spectra. The highly asymmetric line shapes are fitted to the sum of a sharp Gaussian part which is almost resolution limited and a broad damped-harmonic-oscillator shape which extends towards high energies. The final section,

VI, will discuss the results in terms of current theoretical view points and summarize conclusions obtained from the present study.

II. INELASTIC SCATTERING MEASUREMENTS

A. $Mn_{0.5}Zn_{0.5}F_2$

A high-quality single crystal of $Mn_{0.5}Zn_{0.5}F_2$ of about 10 cm^3 in volume was used in the measurement. The Néel temperature T_N determined from the antiferromagnetic (100) Bragg reflection of neutrons was $T_N=21.0$ K. The values of T_N measured at several different spots of the crystal fell within ± 1.0 K of the averaged value, implying a homogeneous Mn concentration of $<\pm 1\%$ deviation throughout the large crystal. A small piece of the crystal cut from the large boule was used in other experiments for critical phenomena and random-field-effect studies reported separately.[7,10] The large crystal was mounted in a He cryostat with its [010] axis vertical to the neutron scattering plane. The inelastic scattering measurements were performed primarily along the [h 0 1] direction from the center ($h=0$) to the boundary ($h=0.5$) of the magnetic Brillouin zone. Limited data in the [001] direction yielded essentially identical results. Most of the data were collected at $T=5.0$ K which is well below the ordering temperature of the crystal.

For the high-resolution measurements at low-energy transfers ($E=0-1.7$ meV) near the zone center ($h=0.0-0.2$), we used a standard triple-axis neutron spectrometer at the H9 cold-neutron source of the high-flux-beam reactor (HFBR) with the final neutron energy fixed at $E_f=3.5$ meV. Contamination of higher-order high-energy neutrons was eliminated from the incident beam by the use of a Be filter. Neutron energy and momentum transfers were defined by a pyrolytic graphite monochromator and analyzer with the collimations of 30′-40′-30′-40′-40′. The instrumental energy resolution for this configuration was about 0.08 meV full width at half maximum (FWHM). This is much better energy resolution than the value of 0.7 meV used in the earlier experiment of Coombs *et al.*[4] This increased energy resolution was made possible both by the increased flux at the HFBR cold source and by the large size of our single crystal.

The intensity of scattered neutrons, $I(q,\omega)$, is proportional to the imaginary part of magnetic susceptibility, $\chi''(q,\omega)$, and to the Bose population factor $\langle n+1\rangle$ as

$$I(q,\omega)=\langle n+1\rangle\chi''(q,\omega)\ , \tag{1}$$

$$\langle n+1\rangle=1/[1-\exp(-E/kT)]\ . \tag{2}$$

The correction due to the magnetic form factor of the Mn ion is negligible in our measurements. The phonon intensity near (001) is negligible in the energy region of our measurements, and the background due to higher-order effects is also quite small. In order to present the shape of $\chi''(q,\omega)$, we divided the observed intensity $I(q,\omega)$ by $\langle n+1\rangle$. At $T=5$ K, for example, $\langle n+1\rangle=1.46$ at $E=0.5$ meV and 1.03 at $E=1.5$ meV. The correction for the Bose factor is important only for low-energy transfers, $E<0.8$ meV.

Figure 2 shows the energy spectra of the magnetic response $\chi''(q,\omega)$ thus measured by neutrons at $T=5$ K for several wave vectors at $h=0-0.2$. The energy spectrum at the zone center, $h=0.0$, shows a sharp peak at $E=0.3$ meV corresponding to the spin-wave energy gap due to the dipolar anisotropy. The line shape is very asymmetric, with a sharp leading edge and a long tail extending towards higher energies. This asymmetric shape will be discussed in Sec. V. With increasing wave vector, the peak position shifts rather slowly towards higher energies, while the width increases very rapidly. As shown in Fig. 2, the line shape at $h=0.2$ is already very broad. This rapid broadening is also reflected in the sharp decrease of the peak intensity with increasing wavevector. It should be noted that the constant background (dotted line in Fig. 2) is very low and the instrumental energy resolution is significantly sharper than the observed broadening. The results in Fig. 2 are thus almost free from resolution correction and represent directly the intrinsic shape of $\chi''(q,\omega)$.

We plot the read-off values of the peak position (PP) and the center of half maximum (CHM) of the energy spectrum versus wave vector h in Fig. 3. Both PP and CHM are measures of the mean energy of the spin waves while CHM accounts in part for the asymmetric shape of the response function $\chi(q,\omega)$. These points in Fig. 3 correspond to the dispersion relation of antiferromagnetic spin waves. For predominant nearest-neighbor interactions, the dispersion relation for antiferromagnetic magnons in a two sublattice antiferromagnet is given simply by[28]

$$E=C[(1+H_A)^2-\cos^2(\pi h)]^{1/2}\ , \tag{3}$$

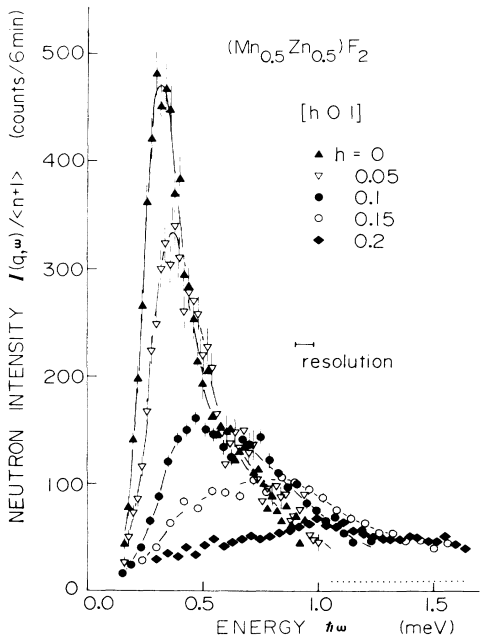

FIG. 2. Energy spectra of spin waves in $Mn_{0.5}Zn_{0.5}F_2$ measured at $T=5$ K along the [h 0 1] direction by use of cold neutrons with $E_f=3.5$ meV. The solid lines are guides to the eye; the dotted line shows the background level.

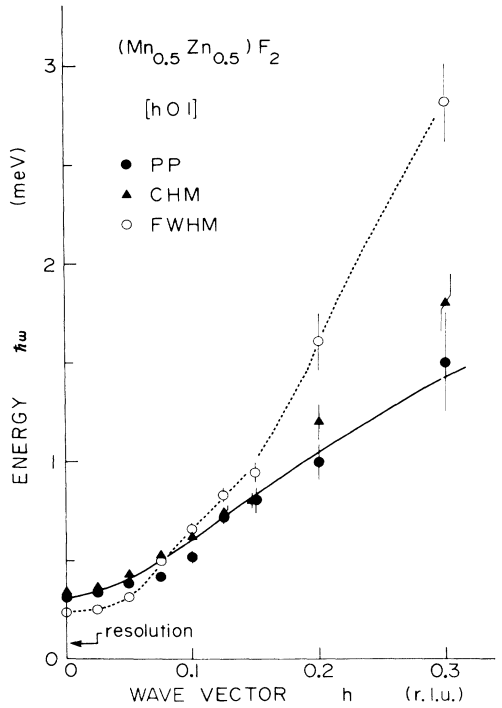

FIG. 3. Dispersion relation of spin waves in $Mn_{0.5}Zn_{0.5}F_2$ measured at $T=5$ K. Peak position (PP), center of half maximum (CHM), and the full width at half maximum (FWHM) read off from the energy spectra are plotted vs wave vector h. The solid line corresponds to the dispersion relation calculated from Eq. (3) with $C=1.7$ meV, while the broken line is a guide to the eye.

where C is the stiffness constant and H_A is the normalized anisotropy field. For $H_A \sim 0$, this equation leads to the well-known linear relation $E=C\pi h$ at small wave vectors $h \sim 0$, and C is the energy at the zone boundary $h=0.5$. The solid line in Fig. 3 represents Eq. (3) with $C=1.7$ meV. We will discuss this value of the stiffness of low-energy magnons in Sec. III.

In Fig. 3, we plot also the full width at half maximum (FWHM) of the energy spectra. At small wave vectors the peak energy is much larger than the full width, indicating that sharp spin waves exist at long wavelengths in this system. With increasing wavevector h, the width becomes rapidly broader, and exceeds the peak energy at around $h \sim 0.15$ reciprocal-lattice unit (r.l.u.). For $h > 0.2$, the FWHM is about 2 times larger than the peak energy. Qualitatively, the excitation is overdamped when the lifetime broadening $1/\tau \sim$ (FWHM)/2 becomes comparable to the mean energy, that is, $1/\tau \simeq E$. In this sense, Fig. 3 demonstrates that the propagating spin waves at small wave vectors h crossover to overdamped excitations at a wave vector of $h_{co}=0.15$ to 0.2.

In general, such broadening of the magnetic excitations can arise either from the spatial geometric randomness of the medium or from thermal effects among the excitations themselves or to both as

$$\Gamma = \Gamma(\text{geometrical}) + \Gamma(\text{thermal}) \ . \tag{4}$$

In pure antiferromagnets, the thermal part is known to depend on temperature T and wave vector q as[29]

$$\Gamma(\text{thermal}) \sim q^2 T^3 \ . \tag{5}$$

By performing inelastic measurements at two different temperatures below T_N, one can check the relative contribution of the thermal effect. Therefore, we took additional data at $T=15$ K; we compare the results with those at $T=5$ K in Fig. 4 for $h=0.1$ as an example. The linewidths at the two different temperatures are almost equivalent. If there were any significant thermal contribution, the width at $T=15$ K should have increased considerably. Figure 4 then indicates that the thermal effect is negligible, and that the observed width is essentially due to the geometrical randomness of diluted spin network.

To explore the excitations at higher energies over the entire Brillouin zone up to the zone boundary $h=0.5$, we extended the inelastic scattering measurement on $Mn_{0.5}Zn_{0.5}F_2$ at $T=5$ K by using thermal neutrons with the fixed incident energy $E_i=13.7$ meV. A standard triple-axis spectrometer was used with a pyrolytic graphite filter, monochromator, and analyzer; the collimations were 20′ throughout. The energy resolution at $E=0$ was about 0.4 meV FWHM, and the resolution become somewhat better at higher-energy transfers due to the fixed incoming energy E_i configuration. The effect of the energy-dependent resolution volume was corrected according to the results of Chesser and Axe,[30] and a constant background 1.8 counts/min was subtracted from the data. In Fig. 5, we present the observed inelastic response $I(q,\omega)/\langle n+1\rangle$ after these corrections. Even near the zone center ($h=0.01$ to 0.1), we observe a substantial amount of excitation extending towards higher energies ($E=3$–6 meV). With increasing wave vector the energy spectra becomes broader, and we see a very flat response at the zone boundary ($h=0.5$).

In antiferromagnets at the zone boundary, the neutron scattering intensity is simply proportional to the energy density of states available for the excitation. Therefore,

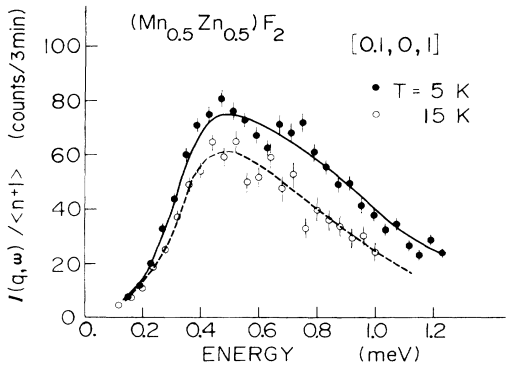

FIG. 4. Energy spectra of spin waves in $Mn_{0.5}Zn_{0.5}F_2$ observed at (0.1,0,1) at two different temperatures $T=5$ K and $T=15$ K below the Néel temperature $T_N=21$ K. The solid and broken lines are guides to the eye. Instrumental energy resolution was much finer than the observed widths, as shown in Fig. 2.

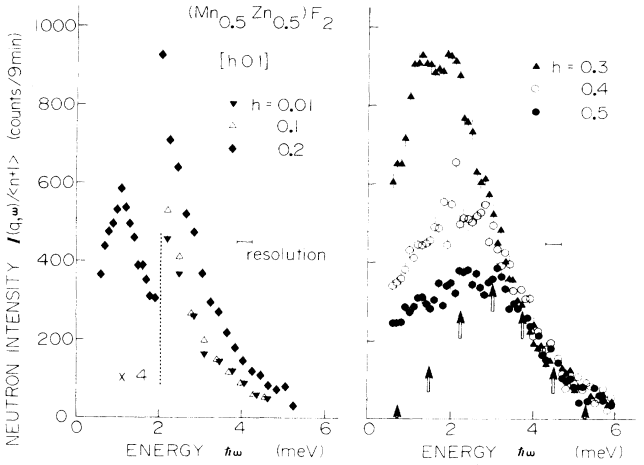

FIG. 5. Energy spectra of magnetic excitations in $Mn_{0.5}Zn_{0.5}F_2$ measured along the $[h\,0\,1]$ direction at $T=5$ K by use of thermal neutrons with $E_i=13.7$ meV. The zone boundary is at $h=0.5$. The arrows show the probability distribution of the net exchange interaction from neighboring antiferromagnetic spins.

we compared the intensity at $h=0.5$ with the probability distribution of the exchange interaction between a Mn spin and neighboring Mn spins on the different sublattice; these are represented by arrows in Fig. 5. This is essentially an Ising cluster model for the zone-boundary response including the finite-cluster contribution. The vertical scale is adjusted arbitrarily so that the response at the higher-energy side overlaps with the arrows. Since the energy resolution (<0.4 meV FWHM) is much finer than the peak interval (~ 0.75 meV), such discrete Ising resonances could have been easily resolved. Resolved peaks close to the energies at the arrows have been predicted by Holcomb and Harris[31] based on a computer simulation using linearized spin-wave theory; such peaks have actually been observed in the case of the two-dimensional diluted antiferromagnets $Rb_2(CoMg)F_4$ and $Rb_2(MnMg)F_4$.[32] In contrast, the observed spectrum in Fig. 5 is rather continuous, although there is a suggestion of some subtle structure similar to that reported by Dietrich *et al.*[5] This demonstrates that the simple Ising-like energy scheme is not adequate to describe the response even at the zone boundary. Moreover, we notice that the observed spectral weight of the low-energy excitations ($E<2.5$ meV) is significantly larger than that expected from the probability distribution. These low-energy excitations will play an important role in lowering the Néel temperature, as will be discussed in Sec. III.

In Fig. 5, it is also evident that the response at higher energies $E>3$ meV does not depend on wave vector for $h=0.2-0.5$. To exhibit this more directly we plot in Fig. 6 the intensity $I(q,\omega)/\langle n+1\rangle$ for several representative energies versus wave vector h. The data from the measurements with cold and thermal neutrons are combined here after normalization for the detection efficiency. This plot corresponds to "constant-E" scans in the language of neutron scatterers. The low-energy excitations at $E<1$ meV show a sharp peak and significant q dependence. In contrast, the intensity at higher energies $E>1.5$ meV exhibits only broad maxima and does not depend significantly on the wave vector. In general, a sharp feature in reciprocal space corresponds to an extended excitation in real space, while a response with no q dependence can be described as "localized" in real space. Here by the word "localized," we simply mean that the excitation is broad both in the energy and momentum; the experiment contains no information on localization in the Anderson sense. (This point will be discussed in Sec. VI.) In this broad sense of localization, the data in Fig. 6 demonstrate that the propagating spin waves at low energies cross over to localized excitations at higher energies $E>1.5$ meV. As a caution, however, we remind the reader that even a paramagnetic spin fluctuation can give rise to a peak at finite q in the constant-E plot like Fig. 6.[33] Therefore, a moderate peak in reciprocal space does not necessarily imply a "propagating" excitation in the strict sense. For the identification of the propagating magnons, one should refer to the relation between the peak energy and the energy width of the energy spectra observed in the constant q scans (see Figs. 2 and 3). In this sense, $E=1.5$ meV given from the constant-E plot of Fig. 6 should be regarded as a safe upper limit for the crossover energy E_{co} above which the excitations are overdamped. Qualitatively, E_{co} can be read off from Fig. 3 as $E_{co}\sim 0.8-1.0$ meV as the energy of the peak position (PP) at the crossover wave vector $h_{co}=0.15-0.2$ r.l.u. A more precise way of determining E_{co} will be introduced in Sec. V.

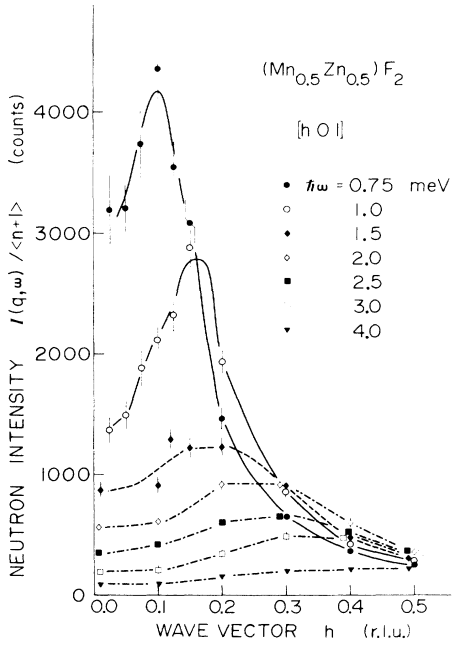

FIG. 6. Magnetic response in $Mn_{0.5}Zn_{0.5}F_2$ at $T=5$ K measured at several different energies plotted vs wave vector h. The solid and broken lines are guides to the eye.

B. $Mn_{0.75}Zn_{0.25}F_2$

We have also performed inelastic scattering measurements on a single crystal of $Mn_{0.75}Zn_{0.25}F_2$ at $T=5$ K in order to provide a foil for the results in $Mn_{0.5}Zn_{0.5}F_2$. The crystal was 4 cm^3 in volume with Néel temperature $T_N=46.2$ K. Some small pieces cutoff from this crystal were used in other experiments reported separately.[7,10] The instrumental conditions were kept similar to those used in the measurements on the 50% specimen. Specifically, we made cold-neutron measurements with a fixed final energy $E_f=2.5$ meV as well as $E_f=3.5$ meV, and thermal neutron measurements with $E_f=13.7$ meV, with collimations equivalent to those described earlier. Sharp spin waves were observed at the zone center with an energy gap of 0.7 meV. In Fig. 7, we plot the read-off values of the peak position (PP) and the width (FWHM) of the energy spectra versus wave vector. The energy width becomes gradually broader with increasing wave vector, but the full width is still much smaller than the peak energy even at the zone boundary. The results in Fig. 7 are generally consistent with those obtained previously by Coombs *et al.*[4] on $Mn_{0.78}Zn_{0.22}F_2$. The dispersion relation of the spin waves in the 75% specimen fits well to Eq. (3) with the stiffness constant $C=3.9$ meV as shown by the solid line.

Figure 7 should be compared with Fig. 3 obtained for the 50% specimen. For $Mn_{0.75}Zn_{0.25}F_2$ spin waves are still well defined at the zone boundary, and there is no indication of any crossover phenomenon. This is in clear contrast with the crossover seen in Fig. 3 for $Mn_{0.5}Zn_{0.5}F_2$. We have also plotted the intensity $I(q,\omega)$ from $Mn_{0.75}Zn_{0.25}F_2$ at several selected energies versus wavevector in Fig. 8. This figure demonstrates that the response at high energies ($E=3-5$ meV) still peaks sharply in reciprocal space. This feature again is in clear contrast with the case of $Mn_{0.5}Zn_{0.5}F_2$ in Fig. 6. These comparisons indicate that the crossover phenomenon observed in $Mn_{0.5}Zn_{0.5}F_2$ is caused by the increased dilution. Specifically, we shall show later that for a dilution of 50% one has begun to enter the percolation regime with a small but measurable percolation correlation length. In the following we shall interpret our data in a percolation picture. It is evident at the outset that more data for samples closer to the percolation threshold $x_p \simeq 0.25$ will be required to confirm this approach. Nevertheless, the predictions of the percolation model are sufficiently successful that we regard this as quite encouraging.

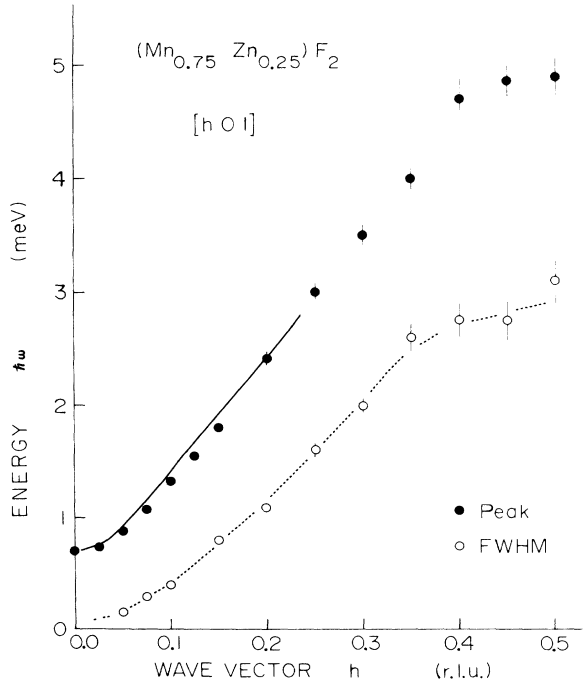

FIG. 7. Dispersion relation of spin waves in $Mn_{0.75}Zn_{0.25}F_2$ measured at $T=5$ K. Peak position and the full width at half maximum (FWHM) of the energy spectra are plotted vs wave vector h. The solid line represents Eq. (3) with $C=3.9$ meV, while the broken line is guide to the eye.

III. PERCOLATION AND THE FRACTON PICTURE

In this section we discuss the experimental results in terms of the percolation problem. For a general review of percolation theory see Refs. 1 and 26. We also provide a brief review of the fracton picture.

A. Spin wave stiffness and the Néel temperature

It is evident that the spin wave stiffness constant $C(x)$ will be reduced from its mean field value $C(x)=xC(1)$ by the ramified geometry of the percolation network. The theory for this is discussed by Harris and Kirkpatrick.[34] Using continuum spin-wave theory they show that for a Heisenberg system

$$C(x)=[A(x)/\chi_\perp(x)]^{1/2}, \tag{6}$$

where $A(x)$ is the exchange stiffness constant and $\chi_\perp$ is

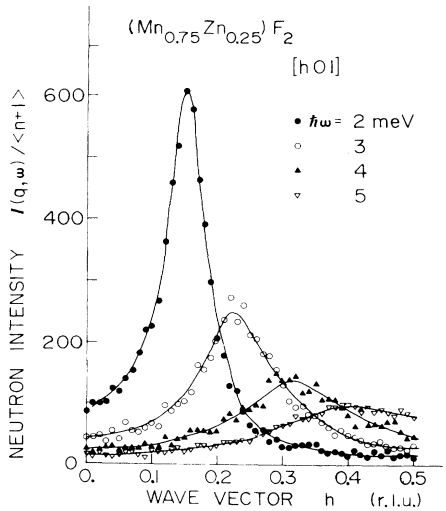

FIG. 8. Magnetic response from $Mn_{0.75}Zn_{0.25}F_2$ measured at $T=5$ K at several selected energies plotted vs wave vector h. The solid lines are guides to the eye.

the transverse susceptibility. This result is also reasonably accurate for small anisotropy. The spin-wave response is controlled by spins which belong to the "backbone" of the percolation network. It has been shown[35] that

$$A(x)/A(1)=\sigma(x)/\sigma(1)\ , \tag{7}$$

where $\sigma(x)$ is the conductivity of the infinite network.

We show in Fig. 9, the population $P(x)$ of the infinite network, $\sigma(x)$ the conductivity, and $C(x)$ the antiferromagnetic spin wave stiffness for the bcc lattice obtained by Harris and Kirkpatrick.[34] For $x=0.5$, $\sim 98\%$ of the spins belong to the infinite network. It is evident, nevertheless, that the percolation geometry already plays an important role since $C(0.5)$ is reduced by nearly a factor of 2 from its mean-field value of $0.5C(1)$. To determine $C(x)$ for our two samples we use the energies given by the center at half maximum (CHM) of the energy spectra for the rather broad response in $Mn_{0.5}Zn_{0.5}F_2$ and the peak position (PP) for the sharp spectra in $Mn_{0.75}Zn_{0.25}F_2$. We then deduce the stiffness constants $C(0.5)$ and $C(0.75)$ from the dispersion relation so obtained; it is evident from Figs. 3 and 7 that Eq. (3) describes the measured dispersion quite well. The values so obtained, normalized to that in pure MnF_2, are shown in Fig. 9; clearly the agreement between experiment and the computer calculations of $C(x)/C(1)$ is very good. It should be noted, however, that the rich structure we see in the measured response $\chi(\mathbf{q},\omega)$ is beyond the scope of this treatment; a more complete modeling of the line shapes will be given in Sec. IV.

An additional feature of the data, which also reflects the low-frequency dynamics, is the Néel temperature $T_N(x)$. In Fig. 9 we plot $T_N(x)/T_N(1)$ for the near-Heisenberg magnet $Mn_xZn_{1-x}F_2$ (Ref. 8) and the isostructural, highly anisotropic Ising magnet $Fe_xZn_{1-x}F_2$ (Ref. 36). In $Fe_xZn_{1-x}F_2$, the reduced Néel temperature is close to $P(x)$ except very near the percolation threshold. In contrast, in $Mn_xZn_{1-x}F_2$, $T_N(x)/T_N(1)$ is greatly reduced. This undoubtedly reflects the enhanced density of low-energy excitations in the near-Heisenberg system. As is evident from the data shown in Figs. 2 and 5, and as we shall discuss in Sec. V, in addition to the low-energy spin waves at long wavelengths there are also low-energy excitations at short wavelengths due to the disordered (fractal?) character of the network. These both will contribute to the diminution of the Néel temperature.

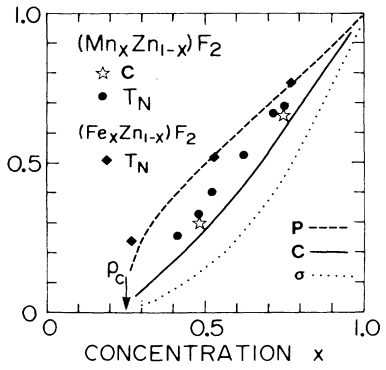

FIG. 9. Concentration dependence of some basic quantities of the percolation network plotted after normalization to the values for the pure system ($x=1$). Population of the infinite cluster (broken line), stiffness constant C of antiferromagnetic spin waves (solid line), and conductivity σ (dotted line) represent the results of Harris and Kirkpatrick (Ref. 34) calculated for the bcc site percolation network. Also plotted are the stiffness constants C obtained from the present experiment on $Mn_xZn_{1-x}F_2$, as well as the Néel temperature T_N of the Heisenberg system $Mn_xZn_{1-x}F_2$ (from Ref. 8) and of the Ising system $Fe_xZn_{1-x}F_2$ (from Ref. 36).

B. Percolation pair connectedness ξ_p

An essential geometrical characteristic of the diluted lattice is the percolation correlation length ξ_p. For $x<x_p$, $\xi_p(x)$ is the average cluster size while for $x>x_p$ it represents the average disconnected cluster size. The spatial spin-correlation function $\langle S(r=0,t=0)S(r,t=\infty)\rangle$ of the spins on the infinite cluster has two components below T_N; a constant part surviving at $r\to\infty$ plus a part decreasing with increasing r with the decay length scale of $\sim\xi_p$. The latter part corresponds to the geometrical short-range spin correlation. As discussed by Birgeneau *et al.*[37] ξ_p is readily measured in magnetic systems from the diffuse scattering around the magnetic Bragg position at low temperatures. Experimentally it is found that the geometrical scattering has an Ornstein-Zernike form

$$S_G(\mathbf{q})=\frac{A}{1+\xi_p^2 q^2}\ , \tag{8}$$

where $q^2=q_x^2+q_y^2+q_z^2$ with the q_α in reciprocal-lattice units. We will present measurements of $S_G(\mathbf{q})$ in $Mn_{0.5}Zn_{0.5}F_2$ in Sec. IV.

C. Fracton picture

As is by now well known, a percolation network provides a prototypical example of fractal geometrical behavior.[11,12,38] Indeed, the nonintegral dimensional behavior of percolation networks was first noted by Stanley *et al.*[38] in 1976 and the essential static geometrical features were discussed by them.

For $x=x_p$, the mass $M(r)$ of the infinite cluster within a sphere of radius r exhibits the behavior

$$M(r)\sim r^D\ , \tag{9}$$

where the fractal dimension $D<d$ the Euclidean dimension. Thus the infinite network has zero density at $x=x_p$. For $x>x_p$ the system is fractal for $r<\xi_p$ and Euclidean for $r>\xi_p$. In three dimensions $D\simeq 2.5$. Heuristically, one might then expect excitations on a diluted spin network with $x>x_p$ to look like ordinary magnons at long wavelengths and to have a fractal character at short lengths.

The dynamics of fractal systems have recently been discussed in detail by a number of authors.[13–18] As noted above, at long wavelengths one expects well-defined excitations with a density of states

$$N(\omega)\sim\omega^{d-1} \quad (r>\xi_p) . \tag{10}$$

By contrast, in the fractal regime, one expects

$$N(\omega)\sim\omega^{2D/(2+\theta)-1} \quad (r<\xi_p) , \tag{11}$$

where θ is a new exponent which measures the range dependence of the diffusion constant on a fractal. The excitations for $r<\xi_p$ thus have an effective dimensionality

$$d_f=2D/(2+\theta) . \tag{12}$$

These excitations at short wavelengths are called *fractons* and d_f is the *fracton dimension.* Alexander and Orbach[13] have noticed that d_f is very close, if not exactly equal to $\frac{4}{3}$. In theories of localization, all excitations are localized in the Anderson sense for $d\leq 2$.[39] Thus the fracton excitations are expected to be localized.[14] Concomitantly, because they are localized the fractons should be observable in a scattering experiment at all wave vectors q.

At the time of writing of this paper, a full theory for the dynamics of magnetic excitations in diluted antiferromagnets for $x>x_p$ is still under development. However, the following general features seem likely to survive further research. At long wavelengths, one expects sharp propagating excitations whose intensity should diminish rapidly as $q\rightarrow\xi_p^{-1}$. For $q>\xi_p^{-1}$, and possibly for all q, one expects broad, localized excitations which are characteristic of the fractal network. Using scaling, Aharony *et al.*[18] derived the Ioffe-Regel criterion thence predicting that for $q>\xi_p^{-1}$ the half-width of the excitation $\Gamma(q)$ should scale linearly with the energy $\omega(q)$ with $\Gamma(q)\sim\omega(q)$. In neutron scattering parlance such excitations are generally referred to as overdamped.

For $q\sim\xi_p^{-1}$, Aharony *et al.* predict that the magnon and fracton contributions to $\chi(\mathbf{q},\omega)$ are additive so that one might expect a two-peaked function. They also suggest that the fracton response should be similar to broadened damped-harmonic-oscillator (DHO) form. A two-peaked response for $q\sim\xi_p^{-1}$ was already suggested by the effective-medium calculations of Orbach and Yu.[40]

In addition to these excitations on the infinite network there will also be local excitations from the finite clusters. In $Mn_{0.5}Zn_{0.5}F_2$ the finite clusters are small in size and contain only a small fraction of the total number of spins. Thus they can be effectively ignored.

IV. DIFFUSE SCATTERING MEASUREMENT

In order to compare properly our inelastic experiments and the theories, it is crucial to determine the pair correlation length ξ_p for $Mn_{0.5}Zn_{0.5}F_2$. As noted above, the elastic scattering at low temperature is given by the Bragg peak from the constant part of the spin-correlation function together with diffuse scattering which represent the geometrical short-range correlation; the latter is described by Eq. (8). We therefore performed an elastic diffuse scattering measurement on $Mn_{0.5}Zn_{0.5}F_2$ with very high-energy resolution. Specifically, a cold-neutron measurement with incident and final energies of 3.5 meV and collimation 30′-40′-30′-40′-40′ was performed. This provides an energy window of $\Delta E\sim 0.08$ meV FWHM. We observed the diffuse scattering intensity at $T=5$ K (well below $T_N=21$ K) along the $[1,0,l]$ and $[1+h,0,0]$ directions around the (100) antiferromagnetic Bragg peak with the [010] axis of the crystal perpendicular to the scattering plane.

To estimate the intensity due to the nuclear incoherent scattering, we performed another measurement at $T=70$ K, well above T_N; here the scattering showed almost uniform intensity with little dependence on wave vector. In Fig. 10, we plot the difference of the observed intensities $I(T=5\text{ K})-I(T=70\text{ K})$ which represents the magnetic diffuse scattering at $T=5$ K. In the transverse scan along $[1,0,l]$ direction shown in Fig. 10(a), we indeed found the anticipated diffuse scattering centered around the (100) Bragg peak. We fit the observed result with Eq. (8) plus a constant. The Lorentzian part corresponds to the exponential decay of the short-range spin correlations in real space while the constant term is presumably due to isolated spins. The observed result fits well to this form with $\xi_p^{-1}=0.15\pm 0.01$ r.l.u. Thus we have determined the pair connectedness ξ_p of the present system $Mn_{0.5}Zn_{0.5}F_2$.

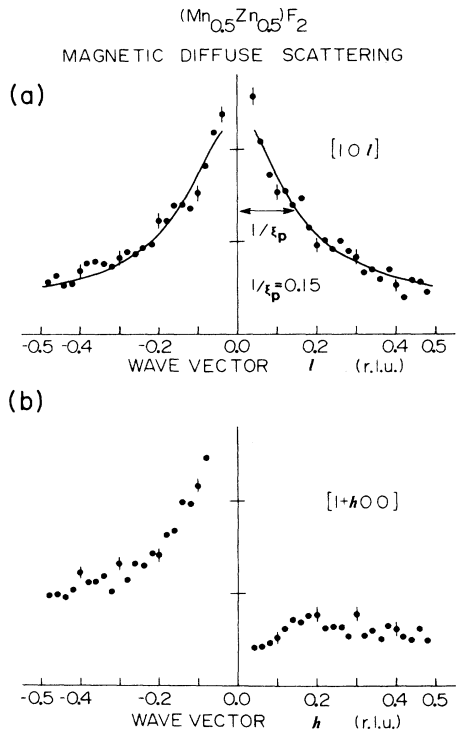

FIG. 10. (a) Magnetic diffuse scattering observed in the transverse scan $[1\,0\,l]$ direction and (b) the longitudinal scan $[1+h\,0\,0]$ direction. The elastic scattering intensity was selected by the energy window $\Delta E=0.08$ meV. Two sets of measurements were performed at $T=5$ K and $T=70$ K, and the difference in intensity $I(5\text{ K})-I(70\text{ K})$ is plotted. The solid line in (a) represents the fit to the line shape with Lorentzian [Eq. (8)] plus a constant.

In the longitudinal scan along the $[1+h,0,0]$ direction, we found an asymmetric profile around (100) as shown in Fig. 10(b). Such scattering is common in alloy systems studied at high resolution. The asymmetry is a manifestation of so-called "Huang scattering"[41] due to the lattice direction wave.[42] In $Mn_xZn_{1-x}F_2$ the lattice constant of an adjacent Mn-Mn pair is slightly different from that of a Zn-Zn pair. This causes a local lattice distortion, and such a distortion propagates as a static strain wave in the crystal. In the tetragonal lattice of $Mn_xZn_{1-x}F_2$ along the [0,1,0] or [0,0,1] directions, the displacement of atoms is parallel to the direction of the propagation, that is the distortion wave is longitudinal. The displacement of Mn atoms gives rise to magnetic diffuse scattering around the antiferromagnetic Bragg point. As described by Krivoglaz,[43] the neutron scattering intensity for this process is proportional to

$$I(q;Q)\sim[\mathbf{n}(\mathbf{q})\cdot\mathbf{Q}/q]^2 , \tag{13}$$

where $\mathbf{q}$ is the reduced wave vector, $\mathbf{Q}$ is the scattering vector, and $\mathbf{n}(\mathbf{q})$ is a unit vector in the propagation direction $\mathbf{q}$ of the displacement wave. It is essential to note that the amplitude of this term is odd in $\mathbf{q}$. The observed scattering in a *longitudinal* scan represents the coherent sum of Eq. (8), Eq. (13), and the nuclear and magnetic incoherent scattering. This will produce an asymmetry such as that shown in Fig. 10(b). No such asymmetry should occur in the corresponding transverse scan where $\mathbf{q}\perp\mathbf{Q}$, in agreement with our experiment, Fig. 10(a). We have not, however, attempted to fit the longitudinal data, Fig. 10(b), to an explicit model for the strain.

In summary, the elastic transverse diffuse scattering measures purely elastic processes which in turn reflect the static geometrical properties of the spin network. For $Mn_{0.5}Zn_{0.5}F_2$ we thus find $\xi_p^{-1}=0.15$ r.l.u. This agrees well with the crossover wave vector $h_{co}\sim0.15$ r.l.u. observed in our inelastic scattering study of the dynamics. This suggests strongly that the crossover phenomena observed in the dynamic measurements are indeed consistent with our expectations based on the fracton picture for the dynamics of a percolation network. To make this comparison more complete, we need to analyze the line shapes themselves.

V. INELASTIC SPECTRAL LINE SHAPES

In this section, we discuss the details of the line shapes of the intensity profile $I(q,\omega)$ observed in the inelastic scattering measurements on $Mn_{0.5}Zn_{0.5}F_2$. As shown in Sec. II, the observed response at small q near the zone center has a highly asymmetric shape with a sharp peak at low energies and a "tail" extending towards higher energies. As discussed in Sec. III Orbach and Yu[40] and Aharony *et al.*[18] have suggested that the response should have two components. Namely, the spectrum may be described as the sum of a sharp component at low energies plus a broad component extending to high energies. It is clear phenomenologically that such a "two-component" shape would in general be useful in explaining the asymmetric line profiles. Therefore, we fitted the observed spectra from $Mn_{0.5}Zn_{0.5}F_2$ with a line shape composed of the sum of the sharp Gaussian shape

$$I_G(\mathbf{q},\omega)=A_G\exp\left[-\frac{(\omega-\omega_G)^2}{2\Delta_G^2}\right] \tag{14}$$

with A_G and ω_G q dependent, plus a broad damped-harmonic-oscillator (DHO) shape

$$I_D(\mathbf{q},\omega)=\frac{A_D\langle n+1\rangle\omega\omega_D\Gamma_D^2}{(\omega^2-\omega_D^2)^2+\omega^2\Gamma_D^2} . \tag{15}$$

The sum, Eq. (14) + Eq. (15), was convoluted with the instrumental resolution function $R(\omega)$ to compare with the experimental data at each different wave vector h. A small Gaussian width $\Delta G\sim0.06$ meV was chosen to fit the sharp magnon spectrum at $h=0$, and then kept fixed in the fits for other wave vectors. We then varied the amplitudes A_G and A_D,[44] peak positions ω_G and ω_D, and the width of the damped harmonic oscillator Γ_D to obtain the best fit. The DHO generally represents the response of a system with its own characteristic energy scale ω_D and damping Γ_D when the system undergoes a forced oscillation with the external frequency ω. The DHO form, Eq. (15), varies as ω for $\omega<\omega_D^2/\Gamma_D$ and ω^{-3} for $\omega\gg\omega_D$; these limiting behaviors have been calculated analytically by Aharony *et al.*[18]

Figures 11 and 12 show the data together with the fitted line shapes. The fits are very satisfactory with the normalized χ^2 ranging between 1 and 2. In Fig. 11, we display the Gaussian and DHO parts independently to illustrate the relative amplitude of the two. The sum of

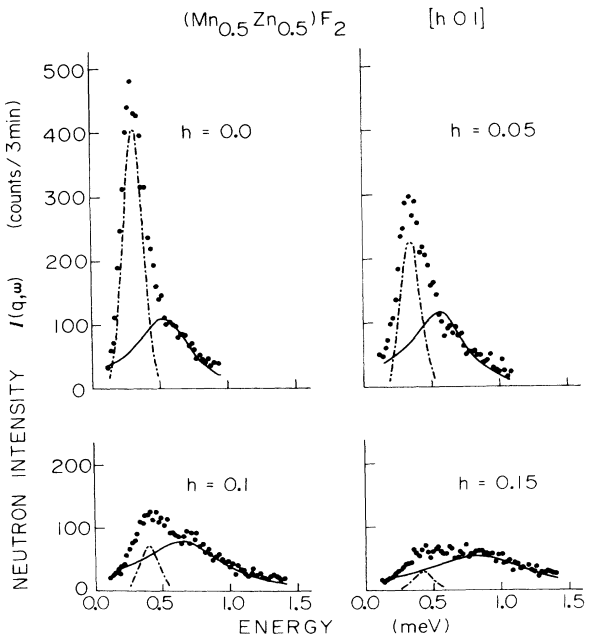

FIG. 11. Energy spectra of magnetic response from $Mn_{0.50}Zn_{0.5}F_2$ at $T=5$ K divided into a sharp Gaussian part [broken line, Eq. (14)] and a broad damped-harmonic-oscillator part [solid line, Eq. (15)]. The sum of the two parts agrees well with the observed data with the normalized χ^2 ranging between 1 and 2.

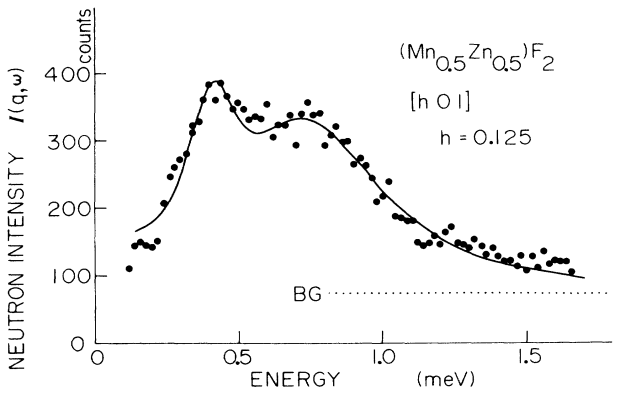

FIG. 12. Energy spectra from $Mn_{0.5}Zn_{0.5}F_2$ observed at wave vector $h=0.125$ r.l.u. in the $[h\,0\,l]$ direction at $T=5$ K. The solid line represents the fit to the sum of Eqs. (14) and (15); the dotted line shows the background level. A double-peak feature characteristic of the wave vector around $h_{co}\sim 0.15$ r.l.u. is demonstrated.

these two components overlaps well with the experimental points. We note that the amplitude of the Gaussian component decreases rapidly with increasing wave vector h. The broad DHO part does not show much dependence on wave vector near the zone center $h<0.15$ r.l.u. Thus the amplitude ratio $A_G:A_D$ plays the principal role in changing the spectral shape with increasing h. At wave vectors around $h_{co}\sim 0.15$ r.l.u., the amplitudes of the Gaussian and DHO parts becomes comparable, and thus we observe a double-peak feature as shown in Fig. 12. At larger wave vectors $h>h_{co}\sim 0.15$ r.l.u., the observed spectra fit well to the DHO shape alone without any sharp component as shown in Fig. 13.

In Fig. 14(a), we plot the peak positions ω_D and ω_G and the DHO width Γ_D versus wave vector. The Gaussian peak energy ω_G increases very slowly with increasing h. The DHO width is smaller than the peak energy ω_D near the zone center. At large wave vectors $h>0.15$ r.l.u. the width Γ_D is about 50% larger than the peak energy ω_D. The strict condition of the "overdamping" of the DHO is $\Gamma_D>2\omega_D$. This, however, should not be interpreted too literally since the functional shape is very broad already for $\Gamma_D\sim\omega_D$ and since the definition for the overdamping is somewhat semantic. We also present the amplitudes A_G and A_D in Fig. 14(b).

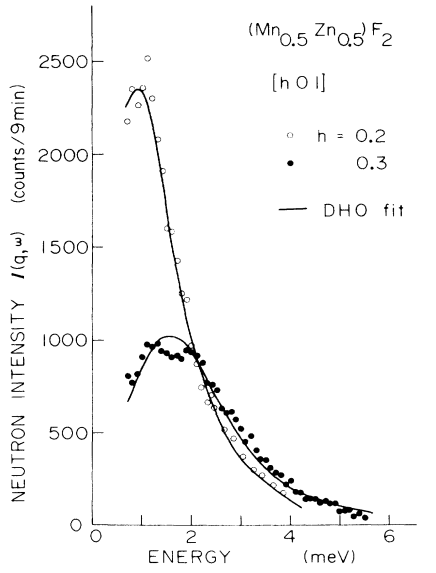

FIG. 13. Fit of the energy spectra from $Mn_{0.5}Zn_{0.5}F_2$ at $T=5$ K to the damped-harmonic-oscillator shape [Eq. (15)] alone.

In the picture discussed in Sec. III, the sharp Gaussian part of $\chi(\mathbf{q},\omega)$ represents the propagating magnons while the broad DHO part is due to the fracton excitations of spins in the ramified region of the network. Since the fracton excitations are essentially localized, there is little q dependence in the DHO part. These features of the line shapes are qualitatively consistent with the theoretical calculation of Orbach and Yu.[40] These authors specifically predicted the double-peak feature at $h\sim h_{co}$. The peak energy ω_D of the broad part at $h\sim h_{co}$ would correspond to the crossover energy E_{co} from low-energy magnons to high-energy fracton excitations. For the present system we identify $E_{co}\sim 0.8-1.0$ meV.

VI. DISCUSSION AND CONCLUSIONS

We have performed an inelastic neutron scattering study of the magnetic excitations in $Mn_xZn_{1-x}F_2$ with $x=0.5$ and $x=0.75$. In the $x=0.75$ sample spin waves exist throughout the Brillouin zone. More interesting behavior is found in the $x=0.5$ sample. In that case we find sharp spin waves near the zone center. With increasing wave vector q, the energy width of the response $\chi''(\mathbf{q},\omega)$ becomes rapidly broader with a crossover around $h_{co}\sim 0.15$ r.l.u. For wave vectors $h>0.2$ r.l.u., the observed full width is about 1.5–2.0 times the average energy scale of the response. By plotting $\chi(\mathbf{q},\omega)$ versus q for several selected energies E, we find that the excitations at higher energies $E>1.5$ meV are very

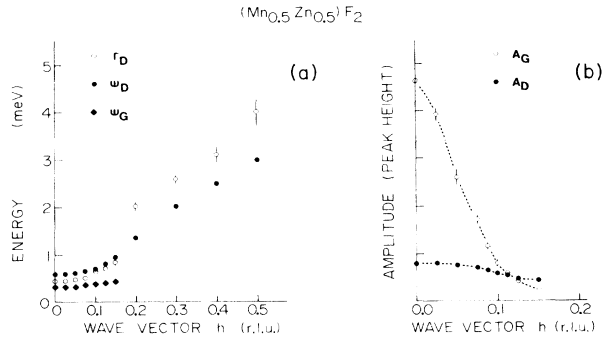

FIG. 14. (a) The best fit values of the peak energy ω_D (ω_G), the energy width Γ_D, and (b) the peak height A_D (A_G) for the damped-harmonic-oscillator (Gaussian) part of the energy spectra from $Mn_{0.5}Zn_{0.5}F_2$ at $T=5$ K. The data at $h\lesssim 0.15$ r.l.u. are fitted to the sum of the two parts, while those at $h>0.2$ r.l.u. are fitted to the damped-harmonic-oscillator shape alone. The dotted lines are guides to the eye.

broad in reciprocal space implying localization in real space.

We also observed elastic diffuse neutron scattering from $Mn_{0.5}Zn_{0.5}F_2$ to measure the characteristic length scale of the spin network. The percolation correlation length ξ_p is determined as $\xi_p^{-1} \sim 0.15$ r.l.u. from the magnetic diffuse scattering observed around the antiferromagnetic Bragg reflection. Thus the crossover from magnons to overdamped excitations occurs around the wave vector $h_{co} \sim \xi_p^{-1}$ given as the inverse of the characteristic length scale ξ_p of the percolation spin network. Recent experiments by Courtens *et al.*[45] on phonons in silica gels suggest similar behavior although their data cover only the long-wavelength regime.

In the $x=0.5$ sample the energy spectra observed near the zone center $h < h_{co}$ exhibit an asymmetric shape with a sharp leading edge and a significant "tail" extending towards the high-energy region. The spectra have been divided into two parts, a sharp Gaussian component which is almost resolution limited plus a broad damped harmonic oscillator shape which covers the high-energy response. The amplitude of the sharp component decreases rapidly with increasing wave vector, while the broad component does not depend significantly on the wave vector. The spectra at short wavelength $h > 0.2$ fit well the DHO shape alone without the sharp component. The sharp Gaussian part is attributed to propagating magnons, while the broad high-energy component would represent the "fracton" response. Near the crossover wave vector $h \sim h_{co}$, the amplitudes of the two components become comparable, and the characteristic double-peak feature is observed. These features of the inelastic line shapes are consistent with the theoretical calculation of Orbach and Yu.[40] The energy width (HWHM) in the short-wavelength region $h > 0.2$ r.l.u. is comparable to the averaged energy scale of the excitation. This is consistent with the scaling theory of Aharony *et al.*,[18] who identify this region as satisfying the Ioffe-Regel condition.

In this paper, we have used the word "localized" in its broad sense to indicate excitations extended both in energy and momentum space. A more strict definition of localization in the transport problem is given as the exponential decay of wave functions with increasing distance. In principle, neutron scattering measures two-spin correlations, while transport properties are determined by four body (current-current) correlations. Therefore, the localization of excitations observed in the present experiment does not correspond directly to Anderson localization in the transport problem. Indeed, theoretical studies to clarify this point would be invaluable.

For the present system of $Mn_{0.5}Zn_{0.5}F_2$, the energy gap of the spin waves at $q=0$ was about $E=0.3$ meV, whereas the peak energy of the Gaussian part at $q \lesssim 0.15$ r.l.u. ranged between 0.3 meV $\lesssim \hbar\omega_G \lesssim 0.5$ meV. The system maintains the basic character of a Heisenberg spin system because the exchange energy is much larger than the anisotropy energy. In this sense, the sharp Gaussian component at long wavelengths can be regarded as arising from the spin-wave excitation. The anisotropy energy, however, makes it difficult to observe directly the linear dispersion behavior expected for the long wavelength magnons in isotropic spin systems. This feature also limit the effectiveness of the direct analogy between antiferromagnetic magnons and phonons. In order to study the detailed dispersion relation of magnons at small q's free from the effect of anisotropy energy, we are planning to perform similar measurements of the spin dynamics in an isotropic diluted Heisenberg system $KMn_xZn_{1-x}F_3$.

Percolation networks are indisputably fractal in character. Thus these diluted magnet experiments provide an unambiguous testing ground for fractal dynamics' ideas. The principal limitation of the current experiments is that the concentration $x=0.5$ is rather far from the percolation threshold $x_p=0.25$ so that $\xi_p^{-1}=0.15$ r.l.u. is a significant fraction of the zone-boundary wave vector $h=0.50$ r.l.u. Thus it is difficult to distinguish the general local character of disordered systems from the direct fractal aspects, especially for the data taken near the zone boundary. We can only say that our results are consistent with expectations based on the magnon-fracton crossover effect discussed by Aharony *et al.*[18] In order to observe the fractal aspect in a wider region of reciprocal space, it is essential to repeat these experiments on several samples with concentrations x approaching to x_p. Such experiments are currently underway both in $Mn_xZn_{1-x}F_2$ and in the two-dimensional square lattice antiferromagnet $Rb_2Mn_xMg_{1-x}F_4$. Other experiments such as NMR, muon spin relaxation,[46] and magnetic specific heat will also be important in probing the fractal dynamics.

ACKNOWLEDGMENTS

We would like to acknowledge stimulating discussions with A. Aharony, R. A. Cowley, J. Kjems, R. Orbach, and G. Shirane. A. Aharony and R. Orbach provided valuable comments on the manuscript. The work at Brookhaven National Laboratory is supported by the Division of Materials Sciences, U.S. Department of Energy, under Contract No. DE-AC02-76CH00016. Research at M.I.T. is supported by the National Science Foundation (Low-Temperature Physics Program) under Contract No. DMR-85-01856.

[1]See, for example, *Ill Condensed Matter*, edited by R. Balian, R. Maynard, and G. Toulouse (North-Holland, Amsterdam, 1979).

[2]See also, *Scaling Phenomena in Disordered Systems*, edited by R. Pynn and A. Skjeltorp (Plenum, New York, 1985).

[3]As a most recent review, see R. Orbach, Science **231**, 814 (1986).

[4]G. J. Coombs, R. A. Cowley, W. J. L. Buyers, E. C. Svensson,

T. M. Holden, and D. A. Jones, J. Phys. C **9**, 2167 (1976).
[5]O. W. Dietrich, G. Mayer, R. A. Cowley, and G. Shirane, Phys. Rev. Lett. **35**, 1735 (1975).
[6]R. J. Birgeneau, R. A. Cowley, G. Shirane, H. Yoshizawa, D. P. Belanger, A. R. King, and V. Jaccarino, Phys. Rev. B **27**, 6747 (1983); D. P. Belanger, A. R. King, and V. Jaccarino, *ibid.* **34**, 452 (1986).
[7]P. W. Mitchell, R. A. Cowley, H. Yoshizawa, P. Boni, Y. J. Uemura, and R. J. Birgeneau, Phys. Rev. B **34**, 4719 (1986).
[8]R. A. Tahil-Kheli and A. R. McGurn, Phys. Rev. B **18**, 503 (1978); D. P. Belanger, F. Borsa, A. R. King, and V. Jaccarino, J. Magn. Magn. Mater. **15-18**, 807 (1980).
[9]R. A. Cowley, G. Shirane, R. J. Birgeneau, and E. C. Svensson, Phys. Rev. Lett. **39**, 894 (1977); G. Aeppli, H. Guggenheim, and Y. J. Uemura, *ibid.* **52**, 942 (1984).
[10]See, for example, R. J. Birgeneau, Y. Shapira, G. Shirane, R. A. Cowley, and H. Yoshizawa, Physica **137B**, 83 (1986), and references therein.
[11]B. B. Mandelbrot, *The Fractal Geometry of Nature* (Freeman, New York, 1983).
[12]See, for example, review articles of H. E. Stanley, in *Scaling Phenomena in Disordered Systems,* Ref. 2, p. 49.
[13]S. Alexander and R. Orbach, J. Phys. (Paris) Lett. **43**, L625 (1982).
[14]R. Rammal and G. Toulouse, J. Phys. (Paris) Lett. **44**, L13 (1983).
[15]P. F. Tua, S. J. Putterman, and R. Orbach, Phys. Lett. **98A**, 357 (1983).
[16]Y. Gefen, Phys. Rev. Lett. **50**, 77 (1983).
[17]S. Alexander, C. Laermans, R. Orbach, and H. M. Rosenberg, Phys. Rev. B **28**, 4615 (1983); O. Entin-Wohlman, S. Alexander, R. Orbach, and K. W. Yu, *ibid.* **29**, 4588 (1984); B. Derrida, R. Orbach, and K. W. Yu, *ibid.* **29**, 6645 (1984); K. W. Yu and R. Orbach, *ibid.* **30**, 2760 (1984).
[18]A. Aharony, S. Alexander, O. Entin-Wohlman, and R. Orbach, Phys. Rev. B **31**, 2565 (1985); A. Aharony, S. Alexander, O. Entin-Wohlman, and R. Orbach, Phys. Rev. Lett. **58**, 132 (1987); and unpublished.
[19]S. Kelham and H. M. Rosenberg, J. Phys. C **14**, 1737 (1981); C. I. Nicholls and H. M. Rosenberg, *ibid.* **17**, 1165 (1984); H. M. Rosenberg, Phys. Rev. Lett. **54**, 704 (1985).
[20]R. C. Zeller and R. O. Phol, Phys. Rev. B **4**, 2029 (1971).
[21]P. Heller and G. B. Benedek, Phys. Rev. Lett. **8**, 428 (1962); V. Jaccarino, in *Magnetism II-A,* edited by G. T. Rado and H. Suhl (Academic, New York, 1965), p. 307; M. P. Schulhof, R. Nathans, P. Heller, and A. Linz, Phys. Rev. B **4**, 2254 (1971).
[22]A. Okazaki, K. C. Turberfield, and R. W. H. Stevenson, Phys. Lett. **8**, 9 (1964).
[23]See, for example, H. Maletta, G. Aeppli, and S. M. Shapiro, J. Magn. Magn. Mater. **31-34**, 1367 (1983).
[24]H. Yasuoka (private communication); M. Ito, Ph.D. thesis, University of Tokyo, 1985 (unpublished).
[25]The diffuse scattering result of the present experiment is a good example. See also Refs. 32 and 37.
[26]D. Stauffer, Phys. Rep. **54**, 2 (1979).
[27]Y. J. Uemura and R. J. Birgeneau, Phys. Rev. Lett. **57**, 1947 (1986).
[28]F. Keffer, in *Handbuch der Physik,* edited by S. Flügge (Springer-Verlag, Berlin, 1966), Vol. 18, p. 1.
[29]A. B. Harris, D. Kumar, B. I. Halperin, and P. C. Hohenberg, Phys. Rev. B **3**, 961 (1971).
[30]N. J. Chesser and J. D. Axe, Acta Crystallogr. Sect. A **29**, 160 (1973).
[31]W. K. Holcomb and A. B. Harris, *Magnetism and Magnetic Materials—1974,* Proceedings of the 20th Annual Conference on Magnetism and Magnetic Materials, AIP Conf. Proc. No. 24, edited by C. D. Graham, G. H. Lander, and J. J. Rhyne (AIP, New York, 1975), p. 102.
[32]R. A. Cowley, G. Shirane, R. J. Birgeneau, and H. J. Guggenheim, Phys. Rev. B **15**, 4292 (1977); R. A. Cowley, R. J. Birgeneau, G. Shirane, H. J. Guggenheim, and H. Ikeda, *ibid.* **21**, 4038 (1980).
[33]Y. J. Uemura, G. Shirane, O. Steinsvoll, and J. Wicksted, Phys. Rev. Lett. **51**, 2322 (1983).
[34]A. B. Harris and S. Kirkpatrick, Phys. Rev. B **16**, 542 (1977).
[35]W. Brenig, P. Wolfle, and G. Dohler, Z. Phys. **246**, 1 (1971); S. Kirkpatrick, Rev. Mod. Phys. **45**, 574 (1973).
[36]G. K. Wertheim, D. N. E. Buchanan, and H. J. Guggenheim, Phys. Rev. **152**, 527 (1966).
[37]R. J. Birgeneau, R. A. Cowley, G. Shirane, J. A. Tarvin, and H. J. Guggenheim, Phys. Rev. B **21**, 317 (1980).
[38]H. E. Stanley, R. J. Birgeneau, P. J. Reynolds, and J. F. Nicoll, J. Phys. C **9**, L553 (1976); H. E. Stanley, J. Phys. A **10**, L211 (1977).
[39]E. Abrahams, P. W. Anderson, D. C. Licciardello, and T. V. Ramakrishnan, Phys. Rev. Lett. **42**, 673 (1979).
[40]R. Orbach and K. W. Yu, J. Appl. Phys. **61**, 3689 (1987).
[41]K. Huang, Proc. R. Soc. London, Ser. A **109**, 102 (1947).
[42]We are grateful to Dr. J. Kjems for kindly pointing out to use the importance of Huang scattering in such measurements.
[43]M. A. Krivolglaz, *Theory of X-Ray and Thermal-Neutron Scattering by Real Crystals* (Plenum, New York, 1969).
[44]In Eqs. (14) and (15), we defined A_G and A_D so that they correspond to the height intensity at the peak position ω_G and ω_D.
[45]E. Courtens, J. Pelous, J. Phalippou, R. Vacher, and T. Woignier, Phys. Rev. Lett. **58**, 128 (1987).
[46]Y. J. Uemura, R. Keitel, M. Senba, R. F. Kiefl, S. R. Kreitzman, D. R. Noakes, J. H. Brewer, D. R. Harshman, E. J. Ansaldo, K. M. Crowe, A. M. Portis, and V. Jaccarino, Hyperfine Interact. **31**, 313 (1986).